ChemInform Abstract: Advanced X-Ray Absorption and Emission Spectroscopy: in situ Catalytic Studies

ARTICLE *in* CHEMICAL SOCIETY REVIEWS · OCTOBER 2010

Impact Factor: 33.38 · DOI: 10.1039/c0cs00054j · Source: PubMed

3 AUTHORS:

Jagdeep Singh
rpc bathinda
17 PUBLICATIONS **451** CITATIONS
SEE PROFILE

Carlo Lamberti
Università degli Studi di Torino
382 PUBLICATIONS **13,153** CITATIONS
SEE PROFILE

Jeroen A van Bokhoven
ETH Zurich
268 PUBLICATIONS **6,123** CITATIONS
SEE PROFILE

Chem Soc Rev

This article was published as part of the

In-situ characterization of heterogeneous catalysts themed issue

Guest editor Bert M. Weckhuysen

Please take a look at the issue 12 2010 table of contents to access other reviews in this themed issue

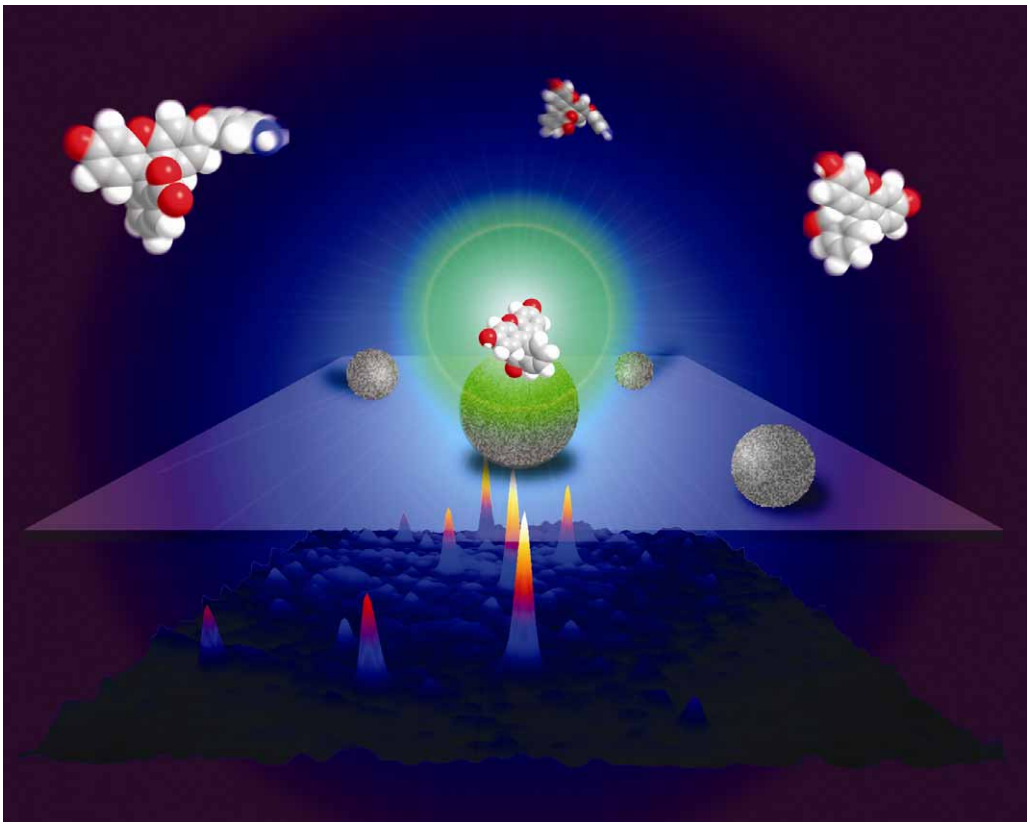

Advanced X-ray absorption and emission spectroscopy: *in situ* catalytic studies†

Jagdeep Singh,[a] Carlo Lamberti[b] and Jeroen A. van Bokhoven*[ac]

Received 26th July 2010
DOI: 10.1039/c0cs00054j

Knowledge of the structure of catalysts is essential to understand their behavior, which further facilitates development of an active, selective, and stable catalyst. Determining the structure of a functioning catalyst is essential in this regard. The structure of a catalyst is prone to change during the catalytic process and needs to be determined in its working conditions. In this *tutorial review*, we have summarized studies done at synchrotron radiation facilities that illustrate the capability to determine catalyst structure using X-ray absorption spectroscopy (XAS) and X-ray emission spectroscopy (XES). These studies aim at facilitating the determination of the dynamic structure-performance relationships during a catalytic process.

1. Introduction

It is essential to know the electronic and geometric structures of materials in order to understand their behavior. Nano-sized particles are of great interest, especially in catalysis where noble metal nanoparticles are often supported on various supports and are used in different reactions such as CO oxidation,[1] the water gas shift reaction,[2] hydrogenation[1d,3] methanation,[4] and hydrogenolysis.[5] The structure of nano-sized particles differs from that of bulk metals. Bulk metals lose their metallic character when the size reduces to less than a few nm.[6] There are many techniques to determine the structure of matter, all with pros and cons; their application depends on the required information and the conditions of measurement. Because of the large penetration depth of X-rays, the interaction of X-rays with matter has been applied extensively. X-ray absorption spectroscopy (XAS) is one of the most popular techniques for determining the structure of materials without long-range order.[7] An XAS spectrum can be divided into three regions, namely the pre-edge, the X-ray absorption near edge structure (XANES), and the extended X-ray absorption fine structure (EXAFS). The shape of XANES spectra gives the electronic structure and the local geometry around the atom that absorbs the X-ray radiation. It reflects the empty density of states (DOS) of the electronic transition. EXAFS spectroscopy provides the coordination geometry, such as bond length (with an accuracy of about 0.01 Å), the number of neighboring atoms, which indicates the size and shape of the nanoparticles, and the Debye–Waller factor.[8]

In an XAS experiment, an electron from a core level is excited through the absorption of a photon of the incoming X-rays. The excited electron is pushed above the Fermi level

[a] *Institute for Chemical and Bioengineering, HCI E 127, Wolfgang Paulistrasse 10, 8093, Zurich, Switzerland. Fax: +41446321162; Tel: +41446325542*
[b] *Department of Inorganic, Physical and Materials Chemistry, NIS Centre of Excellence, and INSTM Reference Center, University of Turin, Torino, Italy*
[c] *Paul Scherrer Institute, Villigen, Switzerland*
† Part of the themed issue covering recent advances in the *in-situ* characterization of heterogeneous catalysts.

Jagdeep Singh

Jagdeep Singh, born and raised in Patiala, India, earned a BE in Chemical Engineering from Thapar University, Patiala in 2004 and a MTech degree in Chemical Engineering from Indian Institute of technology, Roorkee, India in 2006. He completed his PhD under the guidance of Prof. Dr Jeroen A. van Bokhoven in October 2010 at ETH Zurich. His PhD research focused on the exploration of new tools of X-ray absorption and emission spectroscopy for in situ catalytic research.

Carlo Lamberti

Carlo Lamberti: born in 1964; degree in Physics in 1988; PhD in solid state physics in 1993. He is professor in Physical Chemistry at the Torino University since 2006. He has performed more than 100 experiments with synchrotron and neutron sources at ADONE, LURE, ESRF, Elettra, Daresbury, SLS, APS, ISIS, FRM-II, ILL. He has been member of the review committees of ESRF and SLS. His research activities are focused in the multitechnical characterization of nanostructured materials. He edited the book Characterization of Semiconductor Heterostructures and Nanostructures, Elsevier, 2008.

and obtains a kinetic energy equal to the difference in the energy of the incoming X-ray and the bonding energy of the excited electron. As the energy of the incoming X-rays increases, excitation occurs, causing a sharp increase in the absorption signal. This energy is referred to as the absorption edge. XAS is an element-specific technique because the energy of an absorption edge correlates directly to the core-level energy.[9] As the core electron is excited above the Fermi level, XAS reveals information about the unoccupied DOS. For example, the K edge probes the transition of a 1s electron to *n*p and the $L_{2,3}$ edges, that of a 2p to $(n-1)$d. As a result, the L_3 edge is sensitive to the d DOS and directly probes the oxidation state of a transition metal. The first intense feature, also referred to as whiteline, in the L_3 edge spectrum also reveals the anti-bonding state that forms after adsorption of the reactants.[6b,c] The shape and intensity provides information about the electronic and geometric structure of the absorbing atom, and the structure of the adsorption sites of reactants on supported metal catalysts can be determined.[10] The Δμ XANES technique emphasizes these characteristics.[11]

Although XAS and especially EXAFS are well understood and applied experimental techniques along with full theoretical support,[12] they still have limitations. The technique does not distinguish neighboring atoms of similar atomic number such as C, O and N. Furthermore, because an XAS spectrum records the contribution of all the atoms of the selected atomic species present in the sample and gives an average signal, it is difficult to resolve the various geometric and electronic states. This limitation of traditional XAS can be overcome in part by selective XAS. In a traditional XAS experiment, the absorption of X-rays is determined as a function of energy. The core hole created after the excitation of the electron from the core level is filled *via* Auger and fluorescence decay, which can also be measured to determine the absorption signal. With the peculiar experimental set-ups described in Section 5, it is possible to measure the valence-selective XAS by tuning the fluorescence energy of the detector to the energy of a fluorescence line of a particular valence and measuring the XAS signal. This has been done successfully to distinguish the coordination of the two different oxidation states of Fe^{3+} and Fe^{2+} in Prussian Blue.[13] Similarly, spin-selective XAS can be collected by tuning to the high- or low-spin state of an element of interest. Several studies of 3d transition metals[14] have successfully exploited such techniques to reveal the presence of different spin states of the metal under different conditions. Another limitation of XAS is the life-time broadening of the core hole leading to intrinsically broad XAS spectra, hindering a detailed interpretation of the spectra. A partial solution has, however, been found.[14a] A method for recording spectra with smaller life-time broadening will be described in this review (section 2.3).

X-ray emission spectroscopy (XES), a relatively old technique, has strongly developed in recent years due to developments in flux density at third-generation synchrotrons using high-brilliance and tunable X-ray sources.[15] In an XES experiment, excitation can be achieved at a certain energy and the energy-dispersive X-ray emission can be determined by spectrometers based on perfect crystal Bragg optics.[14a,16] Depending on the excitation energy, XES spectra are dependent on or independent of the incident energy, *i.e.* resonant or non-resonant XES. These will be discussed in detail in section 2.1 and 2.2. The general principle of detecting the fluorescence energy of photons, emitted after filling the core hole with valence electrons, is the same for both resonant and non-resonant XES. In contrast to XAS, XES provides information about the occupied orbitals. Because in many cases, both the excited and emitted X-rays are hard X-rays, the *in situ* electronic structure of the specific elements of materials can be investigated.[17] This is in contrast to X-ray photoemission spectroscopy (XPS)[18] and ultra-violet photoemission spectroscopy (UPS),[19] which generally require high vacuum. XES clearly distinguishes ligands such as carbon, nitrogen and oxygen,[20] which is hardly possible with XAS. The peculiarity of the ligand can be revealed, even in the liquid phase when working with organic materials.[21] The technique of resonant XES, also referred to as resonant inelastic X-ray scattering (RIXS) or X-ray resonance Raman spectroscopy, combines XAS and XES.

Here a brief overview of XES is given with a focus on catalysis research. To understand the origin of the activity and reactivity over the catalysts for a specific reaction, the geometric and electronic structures of the ensemble of atoms that form the catalytically active site must be known. Hard X-rays in XES have made dynamic *in situ* measurements possible.

The aim of this review is to guide the reader through typical and recent developments in catalysis, achieved by means of *in situ* XAS and XES. Through presenting a limited number of characteristic examples, the possibilities and limitations will be discussed; concepts and terminology will be presented. Applications of XES for 3d and 5d transition metals will be given, and the instrumentation required to perform XES will be described.

Jeroen A. van Bokhoven

Jeroen A. van Bokhoven was born in 1971 and obtained his degree in chemistry in 1995 and his PhD in inorganic chemistry and catalysis in 2000. Since 2010, he holds a Chair in Heterogeneous Catalysis at the ETH Zurich, Switzerland and is head of the Laboratory for Energy and the Environment at the Swiss Light Source in Villigen, Switzerland. His research interests are heterogeneous catalysis and structural characterization using multiple techniques. New catalysts and catalytic processes are investigated that are related to sustainability.

2. Concepts

2.1 Resonant XES and RIXS

After excitation of an electron from a core level such as 1s, in the case of the K edge, and 2p or 2s, in the case of the L edge, a

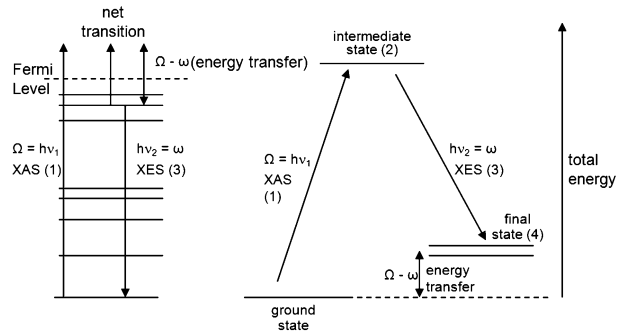

Scheme 1 Orbitals (left) and energy levels (right) showing (1) absorption of an X-ray with incident energy (Ω), (2) generation of the intermediate state, and (3) emission of photon with emission energy (ω). The final state (4) results in energy transfer (Ω–ω).

core hole is generated with a specific life-time broadening. This broadening determines the width of the XAS spectra. The electrons from upper levels decay and fill the core hole, resulting in emission of Auger electrons and fluorescence radiation. With XES, the emitted fluorescence energy is recorded by a high-energy resolution spectrometer. The process, during which the fluorescence energy emitted after the filling of the core hole becomes a function of the incident energy, is referred to as resonant XES or RIXS.[15c,d,16a,22] A RIXS plane is obtained when the incident energy is tuned across an absorption edge, the electronic states are resonantly excited and decay, and the fluorescence is detected in a energy-dispersive manner.[16a] The process is described theoretically by the Kramers-Heisenberg scattering formula.[15d,23] Scheme 1 illustrates the total energy of the RIXS process and the orbital states. As stated above, the RIXS process is a combination of XAS and XES. After absorption of an X-ray with an incident energy $\Omega = h\nu_1$, the ground state electronic configuration is excited into the intermediate state, representing a configuration where the hole is in the core level. This represents the XAS process. Filling the core hole with an electron from one of the upper orbitals generates the X-ray fluorescence with energy $\omega = h\nu_2$. A final state is reached with a hole in the upper orbital. The life-time broadening of this state is less than that of the initial XAS process. This phenomenon is used to record spectra with reduced life-time broadening and higher energy resolution, high-energy resolution fluorescence detected (HERFD) XAS (vide infra Section 2.3).[14a,16] The difference in the energy of the incident photon and that of the fluorescence is the energy that is left in the system, the final state energy or energy transfer ($\Omega - \omega$). These energy diagrams are often translated into contour plots (RIXS planes). Fig. 1 shows the 2p-5d RIXS plane of platinum(IV) chloride (5d transition metal). The RIXS plane clearly shows the two features along the final state energy axis, separated by 3.5 eV. It is noteworthy that RIXS spectra are influenced by the absorption spectral features,[16c,24] because the $2p_{3/2}$ life-time broadening extends along the incident energy of the RIXS plane. This broadening is a fundamental physical property and cannot be eliminated or reduced. From the RIXS plane, different line plots can be deduced along the incident energy axis, energy transfer (final state energy) axis, and along the diagonal. The details of these scans and comparison with the absorption spectra are explained elsewhere.[16b] RIXS is one of the most powerful tools for studying the electronic structure of the transition metal complexes.[25] RIXS is a bulk-sensitive and charge-neutral process, which can be efficiently used to provide site-selective information.[14b,26] RIXS relies on hard X-rays and thus, does not require vacuum. Therefore, high temperature and high pressure do not restrict the application of this technique, making it the perfect tool for catalysis research.[17,27] 1s-2p RIXS has been successfully employed by excitation in the K pre-edge region in 3d transition metals to obtain L edge-like spectra[16b] and provide even more information about the electronic structure than L edge XAS.[22] Thus, RIXS enables the determination of the electronic structure of 3d transition metals with hard X-rays, which has until now been possible only by soft X-ray L edge spectroscopy.[28]

2.2 Non-resonant XES

When the energy of the incoming X-ray is high enough to excite the electron from the core level, well above the Fermi level, it is specifically referred to as non-resonant XES.[16a,22,29] The nomenclature of the fluorescence line depends on the energy level of the electron, which fills the core hole (Scheme 2). The intensity of these fluorescence lines is different from each other. In 3d transition metals, the Kα lines are the most intense. Generally, spin–orbit splitting is not strong enough to separate the 3p energy levels. As a result, the $K\beta_1$ and $K\beta_3$ lines merge and are visualized as a single peak,[16a,30] the $K\beta_{1,3}$ fluorescence line, which is symmetric or asymmetric depending on the transition metal and the type of ligand.[31] Furthermore, there is a small feature at the lower side of the fluorescence energy, known as the Kβ′ line or feature, which in 3d transition metals is assigned to the exchange interaction between 3p and 3d energy levels.[16b,32] Therefore, this feature is rarely, if at all, seen in the compounds with a small valence spin, which further weakens the 3p and 3d exchange interaction. This explains why the Kβ′ feature is not observed in $K_3Fe(CN)_6$ but is observed, with significant intensity, in Fe_2O_3. $K\beta_{1,3}$ and Kβ′ are collectively referred to as the Kβ main lines. Because of this 3p and 3d exchange interaction, the Kβ main fluorescence lines are considered to be an indirect probe of the valence electron configuration in the case of 3d transition metals. Different studies have shown the strong potential of measuring the $K\beta_{1,3}$ fluorescence lines to characterize the oxidation state showing an even better correlation with the oxidation state compared to XANES, which is a standard tool for probing the oxidation state.[33] Kα fluorescence lines, which are approximately eight times stronger than the Kβ main lines, show strong splitting of the $K\alpha_1$ and $K\alpha_2$ lines due to spin-orbital splitting of the 2p levels. Because the interaction of the 2p levels is weaker than that of 3p with the valence levels, the Kα fluorescence lines are a weaker probe of the valence electron configuration in the case of 3d transition metals compared to the Kβ main fluorescence lines. The fluorescence after the decay of an electron from the valence levels of 3d transition metals in order to fill the hole in the core level is $K\beta_{2,5}$ and Kβ″, collectively referred to as Kβ satellite lines.[16b] $K\beta_{2,5}$ indicates the energy of the Fermi level and the Kβ″ feature in transition metal complexes originates from

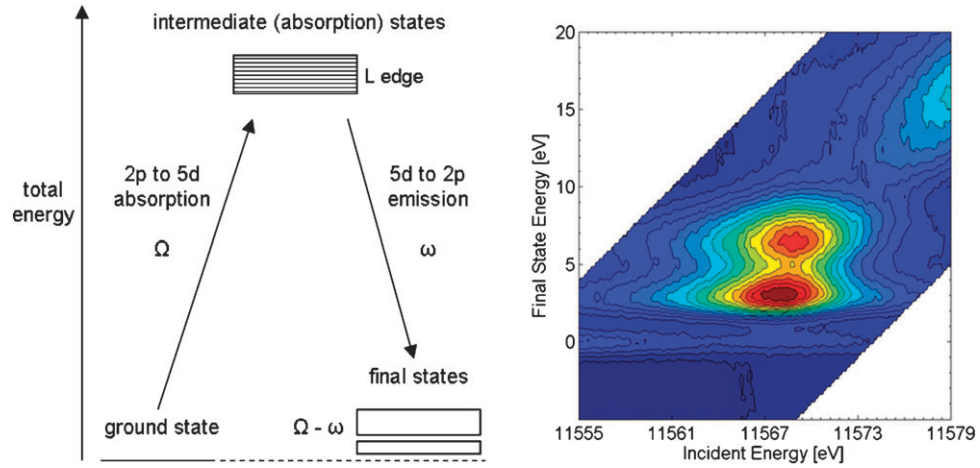

Fig. 1 Total energy with incident and emitted photons (left) and RIXS plane of platinum chloride (right).

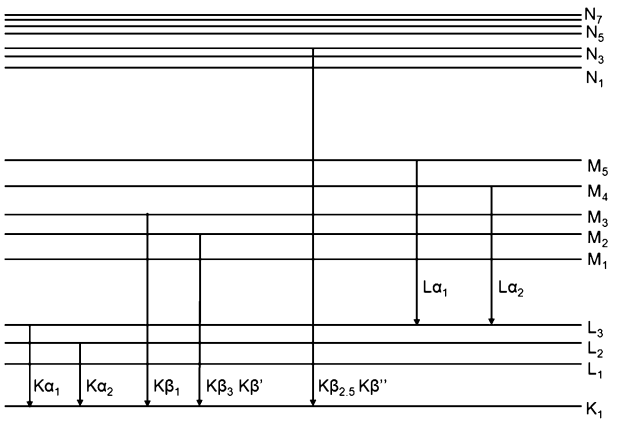

Scheme 2 Energy levels and different fluorescence emission lines.[78]

transitions from the ligand 2s energy levels to the transition metal 1s level.[16b,20,34] As these lines are directly influenced by the valence electron configuration, they are particularly useful for determining the valence electron configuration of 3d transition metals. This, however, is at the expense of sensitivity, because the intensity of the Kβ satellite lines is more than 100 times weaker than that of the Kα fluorescence lines. It is the strong sensitivity of these Kβ″ lines, which makes XES superior to EXAFS in discriminating among ligands with a similar atomic number. To measure the weak $K\beta_{2,5}$ and Kβ″ lines, an X-ray source with high flux and brilliance is required. Third-generation synchrotrons now produce such X-rays, and these methods have developed rapidly.

2.3 High-energy resolution fluorescence detected X-ray absorption spectroscopy (HERFD XAS)

XAS is employed regularly to study the unfilled electronic states above the Fermi level. In a conventional XAS experiment, one monitors the transmitted photons or the radiative and/or non-radiative decay of the sample, while scanning the incident photons. The fluorescence, detected by XAS, is applied to diluted samples which show too little absorption of incoming photons by the element of interest to enable detection of an absorption edge in the transmission signal. The use of Ge detectors with a higher energy resolution than photo-diodes at third-generation synchrotrons with high flux has revealed the structure of diluted samples. There is a limit to the energy resolution set by the life-time broadening of the core hole. To achieve better resolution, it is necessary to circumvent this limitation. This is possible by the selective detection of a fluorescence decay channel, which has a core hole with a longer life-time and, thus, less broadening. This effectively leads to spectra with a higher energy resolution and sharper features.[16,35] Scheme 3 illustrates the spectral sharpening of HERFD XAS, showing the life-time broadening of the Pt $2p_{3/2}$ core level at around 5 eV.[36] The same absorption, which represents the unoccupied states above the Fermi level, can be probed by monitoring a selective fluorescence line such as $L\alpha_1$ ($h\nu_2$ in Scheme 3) which leaves a core hole with a longer life-time (Δt) and, thus, less broadening (ΔE), according to Heisenberg's indetermination principle ($\Delta E \sim h/\Delta t$), see the right hand side of Scheme 3. This technique is also efficient for the fifth row elements of the periodic table, because the final state effects are almost negligible due to the delocalized character of 5d electrons. Care should be taken in the event that the final state effects in resonant excitations close to the

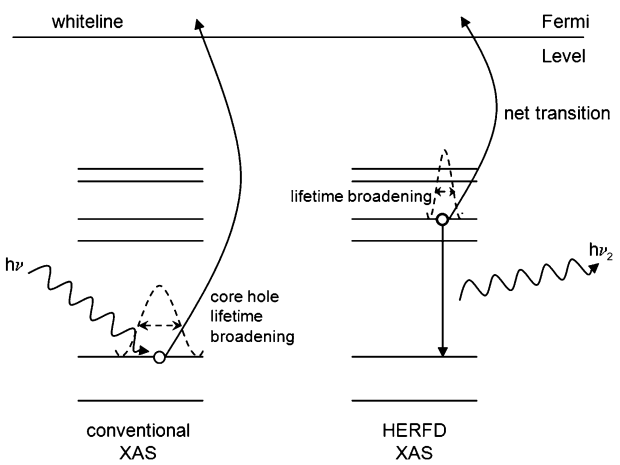

Scheme 3 Orbitals showing electronic transitions and life-time broadening.

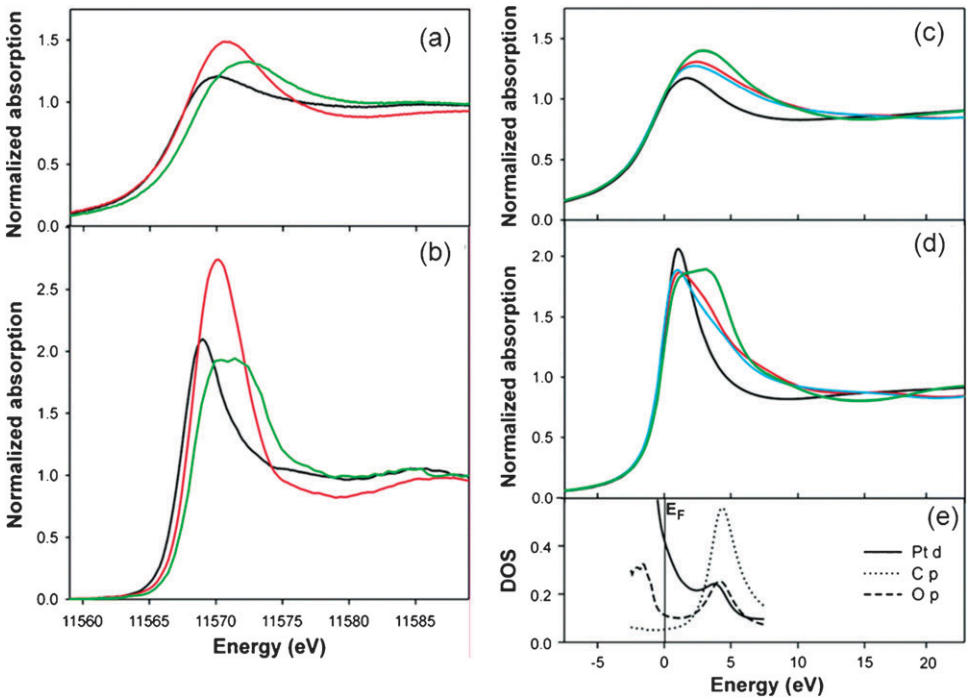

Fig. 2 Pt L_3 edge of 5 wt% Pt/Al_2O_3 after reduction in the presence of different atmospheres: He (black), $He(O_2)$ (red), and 1% CO/He (green) measured using total fluorescence detection (a) and HERFD XAS spectroscopy (b). Theoretical (FEFF8.2) Pt L_3 edge of the Pt_6 cluster (black) and the Pt_6–CO clusters for CO atop (green), bridged (red), and face bridging (blue) with broadening (c) natural and (d) reduced by −1.6 eV; (e) the d-DOS for Pt and p-DOS for C and O calculated for a Pt_6–CO atop cluster.[16c]

Fermi level are significant, because they may result in features in the HERFD scans that may not be real.[24,37] Therefore, in the case of 3d transition metal complexes, special attention should be given to the interpretation of the spectra, because the interactions in the final state are not always weak in the case of the K fluorescence lines. A full theoretical description provides valuable electronic structural information. An improved theoretical description is required to interpret these data. Theoretical calculations, for example, multiplet calculations and FEFF, enable the verification of the features in the HERFD spectra, as has been successfully demonstrated.[16c,d,17,38] Another important advantage of HERFD XAS is that the selective detection of a fluorescence decay channel is element-specific. Thus, HERFD XAS can collect EXAFS spectra with an extended k range, which would be otherwise impossible because of the undesired edges that arise from another element. One of very few examples is the collection of Mn K edge EXAFS in the multiprotein PS II complex.[39] The Fe K edge arises in the EXAFS region of the Mn K edge and limits the distance resolution of EXAFS. HERFD XAS enables the collection of spectra without the Fe edge, which results in better distance resolution and greater precision in the number of metal–metal scattering pairs.

The time needed to acquire XANES and HERFD XANES spectra depends on the energy range to be monitored and the concentration of the absorbing element. Generally, HERFD XANES (Fig. 2b) can be performed in the time range of minutes. For RIXS planes (Fig. 1b), step sizes for final state energy (Y-axis) and incident energy (X-axis) can be varied depending on the features in the planes. Generally, they take hours to be recorded.

3. Applications

3.1 Adsorption studies: catalysis

All catalytic processes proceed in at least three basic steps: (1) adsorption of reactants on the surface of the catalyst, (2) reaction on the surface, and (3) desorption of the products. The structure of an active site is prone to change during the different stages of the catalytic process and must be determined to understand the actual reaction path on the surface of the catalyst. This will facilitate the synthesis of new, more active, selective, and stable catalysts, which often is the basis of catalyst characterization. This section presents the successful application of XAS to study the structure of various catalysts after the first step in the catalytic process: the adsorption of reactants. When an adsorbate is chemically adsorbed on a metal surface, new bonding and anti-bonding states are formed. When the anti-bonding states are pushed above the Fermi level, the adsorbate bonds to the metal.[6a,40] Because L_3 edge XAS probes the empty d DOS, the first intense feature, also referred as the whiteline, and the near-edge structure in L_3 edge spectra are sensitive to the anti-bonding state and to structural changes that occur after adsorption of the reactants or intermediates.[10]

CO oxidation is one of the most studied reactions in the field of heterogeneous catalysis. It is relevant in the automotive catalysis and in the removal of CO from streams of hydrogen used in fuels cells. Therefore, studies of the adsorption of CO on the catalyst surface aid in understanding the key steps in CO oxidation catalysis. HERFD XAS has potential for the identification of the mode of bonding of CO to alumina-supported platinum catalysts.[16c] Combining

experiments with theoretical calculations based on the FEFF code[41] enabled the determination of the dominant CO adsorption configuration on nano-sized platinum and the orbitals involved in the bonding. Fig. 2 shows the spectra collected by means of conventional XAS and of HERFD XAS spectra for an alumina-supported platinum catalyst in different gas environments. The spectral features in the HERFD XAS spectra were significantly sharper[16,35] and showed a higher intensity of the whiteline in the case of oxidized platinum and a doublet feature in the whiteline in the spectrum, which was shown to be typical of CO adsorbed on the surface of the catalyst in atop configuration. The doublet was not resolved in the conventional XAS spectrum. The theoretical calculations confirmed that the CO adsorbed dominantly in the atop position on the platinum surface, which was also known from infrared spectroscopy.[42] Fig. 2 shows the FEFF[41] calculated spectra with three different CO adsorption configurations. The Pt d-DOS overlapped with the $2\pi^*$ orbitals of C and O, resulting in the feature at the higher energy side of the doublet. In bridged and face bridging configurations, the orbitals might not be aligned to overlap sufficiently to form this anti-bonding state.

To complete the determination of the electronic structure, the bonding orbitals and change in the d-DOS of the metal after adsorption of reactants must be determined. Traditionally, XPS[18] of the valence band and UPS[19] are used to probe the structure of the valence band. However, these methods require high vacuum. RIXS, with all its advantages, was employed to gain insight into the occupied d-DOS of platinum upon CO adsorption for alumina-supported platinum catalysts.[17] Fig. 3 shows the $2p_{3/2}$-5d RIXS planes of reduced metallic platinum nanoparticles and the planes of these particles upon adsorption of CO. The features in the RIXS planes show the emission from the d DOS valence band of platinum. For reduced platinum nanoparticles, the elastic peak, the feature at zero energy value of energy transfer, merged with the energy distribution at higher energy transfer. This confirmed that the Fermi level cuts through the 5d band of platinum.[17] The energy resolution was lower than typically observed in XPS and UPS. The energy distribution broadened, and there was a gap between the elastic peak and the occupied states that formed after adsorption of CO. These differences clearly showed the differences in the electronic structure of platinum before and after CO adsorption. Therefore, HERFD and RIXS experiments showed that CO adsorption caused considerable changes in the electronic structure of the platinum catalysts. As the gap opening suggested that the centre of d band shifted away from the Fermi level, it rendered the platinum catalyst to weaker adsorption of reactants.[6a,43] Because according to d band theory, metals that have their d band centre closer to the Fermi level are more active towards the adsorption of adsorbates than those with a d band centre farther from the Fermi level.[6a,43] Therefore, CO poisoned the catalyst not only by occupying the sites but also by lowering the adsorption of other reactants.[44]

Both HERFD XAS and RIXS were also applied simultaneously to study the alloying of platinum nanoparticles with tin.[27a] Alloying platinum with tin resulted in the narrowing of the d band of platinum and a downward shift relative to the Fermi level. The adsorption of CO resulted in a considerable modification of the electronic structure. The strong similarity of the RIXS planes and the HERFD spectra collected after CO adsorption of both the monometallic platinum and bimetallic platinum-tin nanoparticles suggested that the strong adsorption of CO altered the geometric structure of the bimetallic nanoparticles.

3.2 *In situ* studies: catalysis

3.2.1 CO oxidation. Hard X-rays make XES one of the best techniques for studying the electronic structure of catalysts, element specifically, under real reaction conditions. The combination of HERFD XAS and kinetic measurements during CO oxidation over alumina-supported platinum catalysts gave information about the active species in the reaction.[44] They were assumed to be metallic platinum,[45–47] oxidic platinum,[48] or a combination of metallic and oxidic phases[49,50] The oxidation of CO over platinum catalysts occurs in two distinctive regimes namely low- and high-activity regime with low and high rate of CO oxidation respectively.[44,45,47,48,51] Fig. 4 shows *in situ* Pt L_3 edge HERFD spectra, collected during CO oxidation. The spectra established the structure of the catalyst in two different reaction regimes. The spectra in the low-activity regime (at low temperature) showed the doublet in the whiteline, which is characteristic of adsorbed CO on reduced platinum.[16d] The adsorbed CO poisoned the catalyst surface (vide supra) and rendered the catalyst less active.[1c,52] The rate-limiting step, in this regime, is desorption of CO. The spectra collected in the high-activity regime showed an intense whiteline, which is characteristic of partially oxidized platinum.[16d] Quick EXAFS, collected during the switch between the two regimes showed that oxidation of the catalyst occurred during activation.[44,53] The structure of the surface platinum oxide was highly defective with platinum under-coordinated to oxygen.[51e] Therefore, the high-activity regime was characterized by the presence of an active surface oxide.[48,54] The transition from the low-activity regime to the high-activity regime resulted in depletion of CO from the platinum surface, which enabled the oxygen interaction and the formation of the more active catalyst, where the platinum surface was partially oxidic. This enhanced the catalytic activity by changing the rate-limiting step.

3.2.2 Selective oxidation. Another study, the first of its kind to be reported, stressed the advantage of detecting secondary radiation and involved the well-known framework-substituted FeZSM-5 catalyst.[55] Such a catalyst is very selective in the oxidation of benzene to phenol in the presence of N_2O.[56] The activity of the catalyst was strongly dependent on the iron loading and the structure of the active iron species on the method of preparation. Because of the very low iron content, it is difficult to determine the active species of the framework-substituted FeZSM-5 catalyst compared to over-exchanged Fe/ZSM-5, where most of the iron active species have been claimed to be in the form of binuclear iron clusters,[57] similar to active methane monooxygenase in enzymes. The activation processes involving ion-exchange, calcination, and steaming can lead to the formation of different kinds of oxo-iron species. Attempts were made to specify the active species by

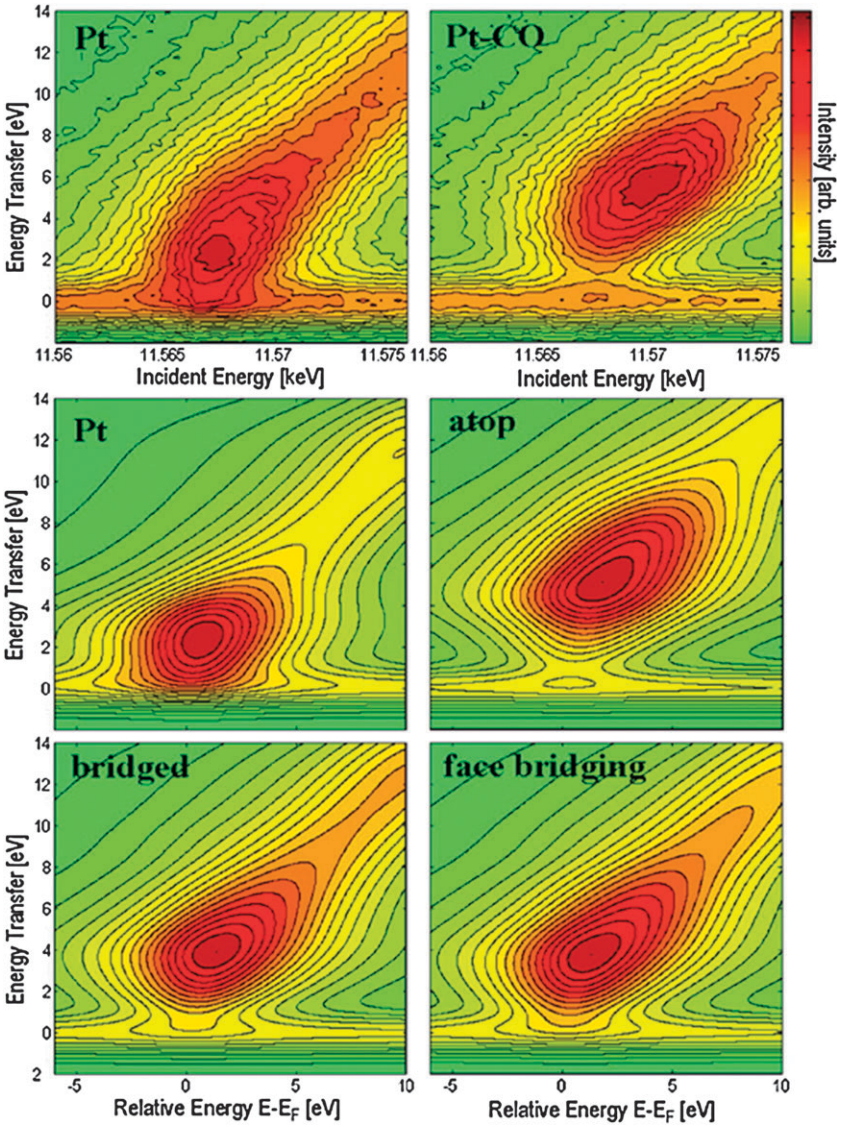

Fig. 3 (top) $2p_{3/2}$ RIXS planes of supported Pt nanoparticles: (left) metallic and (right) with CO adsorbed. (bottom) Calculated RIXS planes for a bare Pt_6 cluster and the cluster with CO coordinated at three different sites. (top) $2p_{3/2}$ RIXS planes of supported Pt nanoparticles: (left) metallic and (right) with CO adsorbed. (bottom) Calculated RIXS planes for a bare Pt_6 cluster and the cluster with CO coordinated at three different sites.[17]

Mössbauer spectroscopy[58] and ESR spectroscopy.[59] The heterogeneity of the active iron-oxygen species and the non-quantitative aspect of the mentioned techniques make the characterization of the catalyst a challenging task. XAS was employed to correlate the structure of iron in terms of oxidation state and coordination of iron silicates.[59,60] The pre-edge region in K-edge XAS spectra is a measure of symmetry and oxidation state. However, subtraction of the main edge from the pre-edge requires appropriate methods to correctly assign the trends. The Kβ-detected XAS spectra, collected by detecting the intensity of the $K\beta_{1,3}$ fluorescence line as a function of incident energy,[16a,22,25a] had sharper spectral features than conventional XAS spectra (vide supra Section 2.3). This aided the better isolation of the pre-edge region, which further facilitated the quantitative determination of the electronic and geometric structures of active iron species in FeZSM-5 catalyst. Fig. 5 shows the Fe K pre-edge feature, determined in conventional mode and selectively by detecting the $K\beta_{1,3}$ fluorescence line. The features were clearly sharper in the Kβ-detected XAS. Moreover, the pre-edge region was virtually isolated from the main edge. Therefore, no background subtraction was required, as was the case with the conventional method. Fig. 6 shows the Kβ-detected XANES of the FeZSM-5 catalyst after different treatments during activation of the catalyst. All the spectra were measured at 350 °C in a flow of 7.7% O_2 in He. An intense single peak in the pre-edge region implied the presence of iron in tetrahedral symmetry.[55,59] In octahedral symmetry, the pre-edge feature is accompanied by a small shoulder. The energy and intensity of the pre-edge feature are the basis for assigning the structure.[61] Iron oxide phases, FeO_x, which are considered to be inactive,[62] were virtually absent, because the centroid of the pre-edge feature, after all the treatments, was closer to the 3+ oxidation state (Fig. 7). The decreasing intensity of the pre-edge

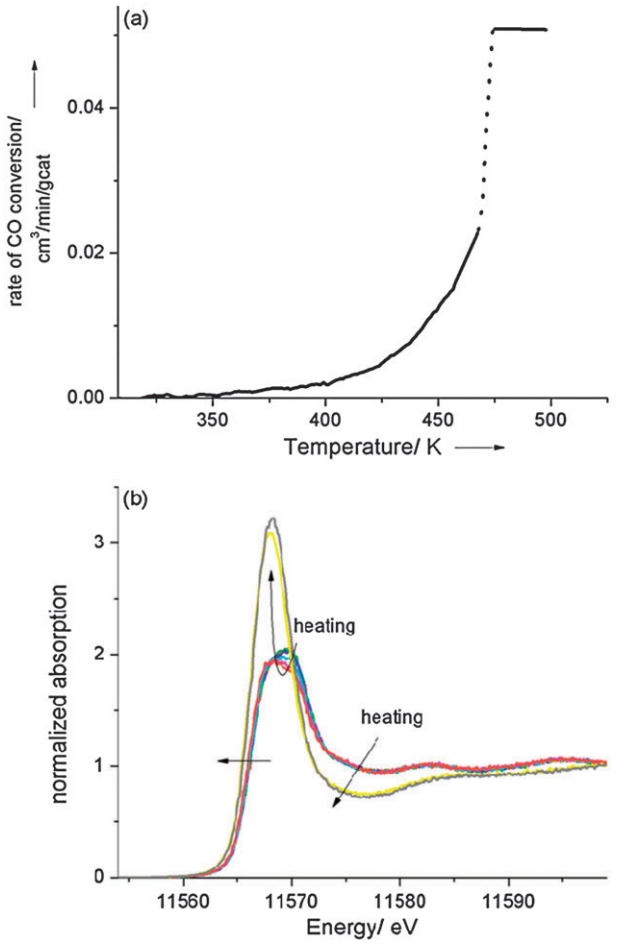

Fig. 4 (a) Rate of oxidation of carbon monoxide over 2 wt% Pt/Al_2O_3 during heating (5 K min^{-1}) at oxygen to carbon monoxide ratios of 1. (b) Pt L_3 edge HERFD XANES of 2 wt% Pt/Al_2O_3 during oxidation of carbon monoxide at an oxygen to carbon monoxide ratio of one measured during heating at 308 K (red), 328 K (green), 361 K (blue) 394 K (cyan), 425 K (pink), 443 K (orange), 475 K (yellow), and 491 K (grey). The arrows indicate the trends.[44]

feature following steaming (Fig. 6) revealed that these treatments extract iron from the zeolite framework and that iron then migrated to extra-framework positions. Kβ-detected XANES gave greater insight into the structure of FeZSM-5 catalysts under *in situ* conditions of activation.

4. Soft X-rays

The energy of soft X-rays is lower than 1000 eV. The absorption K edges of C, N, and O, which are abundant atoms in reacting species, fall in the soft X-ray range. Moreover, the L edges of the first row of elements in the periodic table are in this range. This opens the possibility to look to both adsorbate and catalytic surface. Determining the structure of adsorbate on different transition metals, measured by soft XES, has contributed to understand how these species adsorb and react with the surface. Using grazing incident radiation, the XES technique can be made surface sensitive.[15e] There are many surface-sensitive spectroscopic techniques for studying the electronic structure of adsorbates,[63] but XES enables to

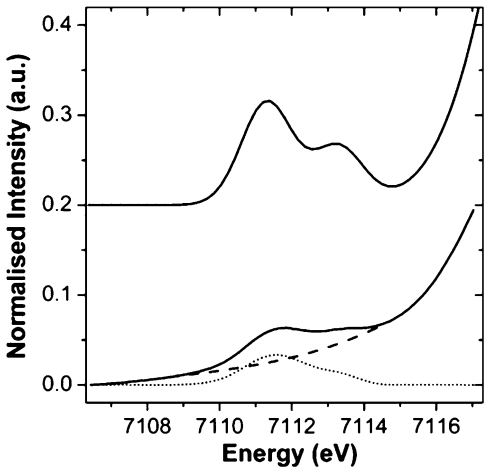

Fig. 5 Fe K pre-edge feature of Fe_2SiO_4 (fayalite: Fe^{II}, O_h). Below: conventional fluorescence XANES spectrum (solid), cubic spline function used to model the background (dash), and the isolated pre-edge (dot). Top: Kβ-detected XANES spectrum, no background subtracted.[55a]

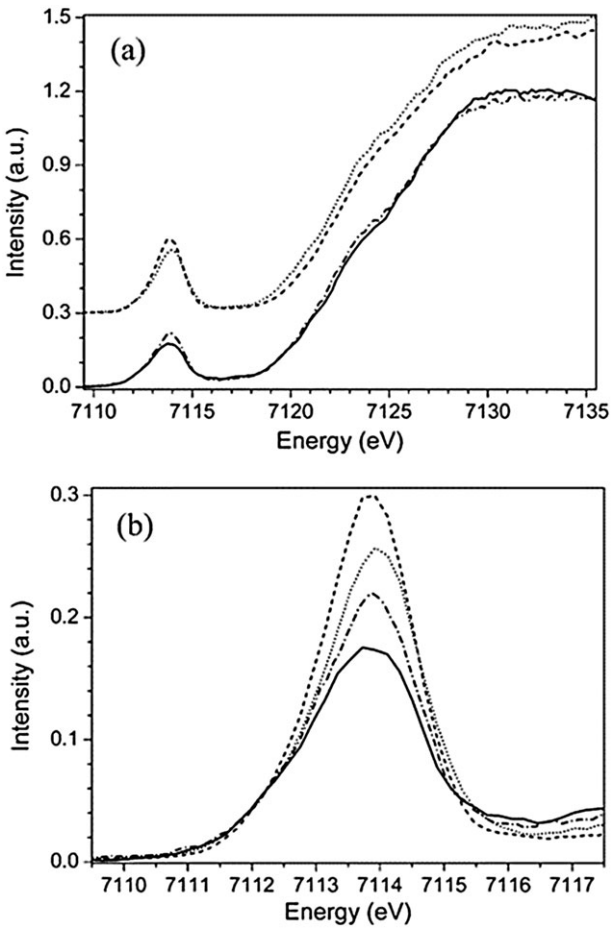

Fig. 6 (a) Kβ-detected XANES of framework-substituted FeZSM-5 samples: *tf*-FeZSM-5, after template removal (dashed line); *H*-FeZSM-5, proton form after calcination of ammonium-exchanged sample (dotted line); *ms*-FeZSM-5, mild-steamed sample (dash-dot line); and *hs*-FeZSM-5, hard-steamed sample (solid line). (b) Zoom of the pre-edge region.[55]

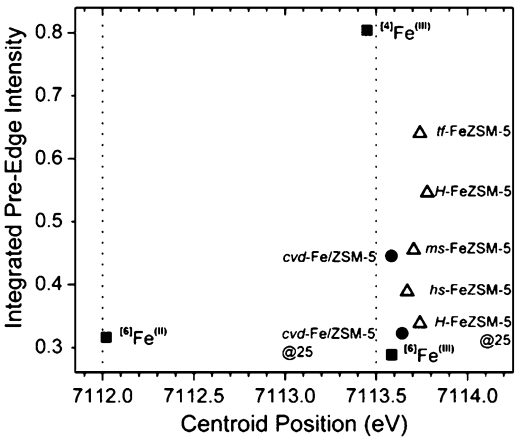

Fig. 7 Integrated pre-edge intensity *vs.* centroid position for iron in different FeZSM-5 samples. Framework-substituted FeZSM-5 samples are compared with extraframework *cvd*-Fe/ZSM-5 samples. All iron-containing ZSM-5 samples are measured in a flow of oxygen (7.7 vol% in He) at 350 °C unless indicated by @25, meaning 25 °C: *tf*-FeZSM-5, after template removal; *H*-FeZSM-5, proton form after calcination of ammonium-exchanged sample; *ms*-FeZSM-5, mild-steamed sample; and *hs*-FeZSM-5, hard-steamed sample. The pre-edge characteristics are also given for iron model compounds: $FePO_4$ = $^4Fe^{(III)}$, α-Fe_2O_3 = $^6Fe^{(III)}$, and Fe_2SiO_4 = $^6Fe^{(II)}$.[55]

determine the electronic structure element specific.[64] XES is, thus, an ideal tool for determining the nature of the surface chemical bonds of molecular adsorbates, such as N_2, CO[65] and hydrocarbons[66] as the structure of either atom can be probed using high energy-resolved X-rays. These studies elucidated the orientation of the molecules on the surfaces and identified the orbitals that are involved in the bonding.

Adsorption of CO

The adsorption studies of adsorbates like N_2 and CO on various transition metals provide a simple and general platform for understanding the processes and phenomena on surfaces and are therefore of great significance in the field of catalysis. Many studies consider the adsorbate as a single molecular unit and weakening of molecular bond is related to the increased electronic population of the anti-bonding 2π* state due to back donation by the metal.[67] Soft X-ray XES enables detecting the orbitals involved in the bonding. CO was shown to adsorb on Ni (100) surfaces preferably on on-top sites with the carbon atom attached to the surface.[68] Fig. 8 compares the XES spectra of adsorbed CO on Ni (100) and Cu (100) surfaces with that of the gas phase CO. The spectra were plotted on the common binding energy scale relative to the Fermi level.[69] The spectra were divided into states of π- and σ-symmetry that were obtained by detecting in the normal and grazing X-ray emission modes respectively.[70] For gas phase CO, such division was not possible. These experimental XES spectra were well reproduced using ground-state calculations obtained by density functional theory (DFT) calculations,[65] as shown in Fig. 9. In Fig. 8, the 1π state of the free CO molecule had a much higher intensity in the O K edge emission spectrum compared to that of the C K edge. This indicated that the polarization is mainly towards the oxygen atom

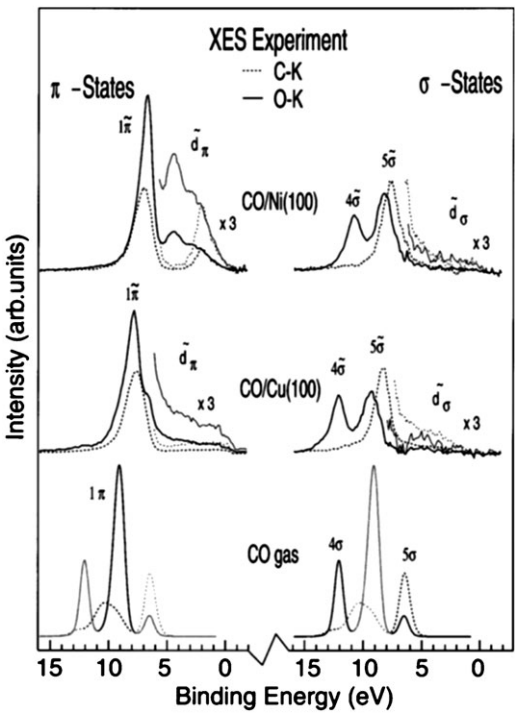

Fig. 8 Experimental X-ray emission spectra of the carbon and oxygen atomic centers (*K*-edges) for CO gas and adsorbed CO on Cu(100) and Ni(100). The adsorbates have a *c*(2×2) superstructure on the crystal (100) faces, occupying on-top sites.[65]

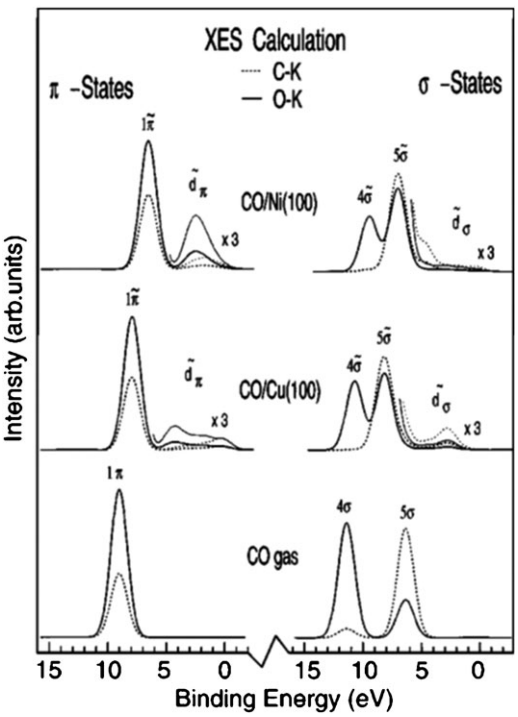

Fig. 9 Ground state frozen orbital calculations of carbon and oxygen *K*-edge XES for CO gas and CO adsorbed on Cu_{26}- and Ni_{13}-cluster models. Broadening of 0.5 eV (FWHM).[65]

within the CO molecule. After adsorption of the CO on either Ni (100) or Cu (100) surface, the 1$\tilde{\pi}$ is less polarised towards

O as the ratio of the intensities of O to C emission peaks decreased. For both Ni (100) and Cu (100) surfaces, the broad features originated between the Fermi level and 5 eV in the π-symmetry state spectra (shown in the zoom on the left side of Fig. 8). These were assigned to the $\tilde{d}_{\pi}$-band state because these states arose mainly from the metal d-band.[65] The $\tilde{d}_{\pi}$-band had some differences for Ni and Cu surfaces. For Ni (100) surface, the feature at about 4.5 eV was clearly visible only in the O K edge spectrum. This state is a characteristic oxygen lone-pair of π-symmetry.[65] The feature at 1.5 eV had contributions from both O and C K edge spectra. For Cu (100) surface, similar spectral features were observed but they were less pronounced. The O K edge spectrum had a broad distribution tailing towards the Fermi level, which was centered around 5 eV. The C K edge spectrum distribution had always lower intensity compared to O K edge spectrum. These differences between Ni and Cu could be assigned to the fact that in Cu the energetic mixing of p-band with d-band is not as favorable as in Ni. This leads to a broad energetic spread of $\tilde{d}_{\pi}$-band state for Cu compared to Ni.

Fig. 8, right side shows the experimental XES spectra of σ-symmetry are shown. The 4σ and 5σ states that represent the two occupied outer valence orbitals of σ-symmetry changed in peak position and in relative intensities after adsorption of CO as indicated by $4\tilde{\sigma}$ and $5\tilde{\sigma}$ states. The relative strength of $4\tilde{\sigma}$ and $5\tilde{\sigma}$ states in O K edge spectrum is the measure of the degree of polarization upon adsorption. For gas phase CO, in the O Kedge spectrum, the relative intensity of 4σ is higher than that of 5σ state. But, after adsorption of CO on Ni (100), the relative intensity of 4σ became less than 5σ state, and after adsorption of CO on Cu (100), the intensities were almost similar. Also the relative energy positions of $4\tilde{\sigma}$ and $5\tilde{\sigma}$ states changed as this difference was decreased to 2.5 eV compared to 5.5 eV for the gas phase CO. These differences suggested polarization of the $5\tilde{\sigma}$ towards the oxygen atom and the $4\tilde{\sigma}$ towards the carbon atom after adsorption of CO on either metal surface. There were some weak features tailing towards the Fermi level assigned to the d_{σ} band.

These spectra showed how the adsorbate electronic structure was changed after the adsorption of CO on the metal surface. These changes strongly effect the bond formation between the adsorbate and the metal surface. Table 1 summarizes experimental and theoretical values of the C–O stretch frequency, C–O bond distance, C–Me bond distance, and the adsorption energy of gas phase CO and CO adsorbed on Cu (100) and Ni (100) surfaces. The change in the adsorption energy directly indicates the overall stability of the system and the C–O stretch frequency, C–O bond distance, and C–Me bond distance can be used as the parameters to describe the local bond characteristics. By applying constrained space orbital variation analysis,[71] and analysing the change in C–O stretch frequency, C–O bond distance, and C–Me bond distance, upon changing the π- and σ-symmetry orbitals individually, it was concluded that π- and σ-symmetry orbitals behave opposite to each other. The mixing of the π-symmetry orbitals of CO with the metal weakens the internal CO bond and favours the metal CO bond formation whereas σ-symmetry orbitals gives a repulsive contribution to the metal CO bond and thus leads to strengthening of the internal CO bond. Therefore, the overall result of these polarizations between the CO molecule as observed in the XES spectrum and the π- and σ-interaction is the partial breaking of the internal bonds of CO and formation of metal CO bond.[40]

5. Instrumentation

XES proceeds by the selective collection of emitted photons from the sample. Various types of XES spectrometers exist. With one type of spectrometer, scanning occurs through the desired energy range along the Bragg angle, and the crystal used in such spectrometer is referred to as the Bragg crystal. It is generally a spherically bent crystal[16b,72] which increases the efficiency of the spectrometer in collecting all the fluorescence lines from the sample with the same Bragg angle. To achieve this, the sample, the Bragg crystal, and the detector all need to be in Rowland geometry. This type of setup was first introduced by Johann[72a] (Johann-type spectrometer). The energy resolution of such spectrometers depends for most part on the quality of the crystal and also on the deviation from the Rowland geometry.[72c] The photon efficiency of such spectrometer can be increased by increasing the number of crystals that are all aligned on a Rowland circle. Such setups are already existing at various beamlines at synchrotron radiation facilities *e.g.* ESRF, SSRL, and SLS. The detectors are generally solid-state[72a,c,73] or MYTHEN-II detectors.[74] The type of Bragg crystals depends on the energy range of the XES study and their number and size effect the sensitivity.

Another type of spectrometer design is based on polychromators, which are either flat crystals[75] or cylindrically bent crystals.[76] Because the crystal causes a polychromatic dispersion of the fluorescence X-rays from the sample, a position-sensitive detector is required in this type of spectrometer. It is not required to scan the Bragg angle across the spectral range, so that such polychromatic spectrometers are more suitable for the simultaneous recording of all parts of the spectrum and are at the forefront of time-dependent studies. However, due to the lower energy resolution of the detectors and the lower signal-to-noise ratio because of unwanted scattering, polychromatic spectrometers are not as suitable

Table 1 CO ground state properties from experiment and calculations[65]

	C–O stretch frequency/cm^{-1}		d C–O, D C–Me/Å		E_{ads} (eV/molecule)	
CO properties	Theory	Experiment	Theory	Experiment	Theory	Experiment
Gas	2101	2169.8	1.146	1.128		
Cu (100)	2049	2089.0	1.161, 1.950	1.15 ± 0.10, 1.90 ± 0.10	−0.6	−0.7
Ni (100)	1976	2064.8	1.165, 1.749	1.13 ± 0.10, 1.80 ± 0.10	−1.7	−1.3

as spectrometers based on Bragg crystals in Rowland geometry. The combination of both spectrometers and performing dispersion-compensation correction led to a much better energy resolution without any loss in the accepted solid angle.[77]

6. Conclusions

XES is a powerful tool for studying the electronic structure element specific. The high-energy resolution achieved by selective detection of a fluorescence channel is employed to study the behaviour of supported metal catalysts under actual catalytic conditions (high temperature and various gases). Such measurements play a vital role in following a reaction over a catalyst surface as the structure of the surface sites can be probed efficiently with better resolution compared to conventional XAS technique. RIXS is utilized in *in situ* studies to determine the active species of catalysts. The knowledge gained from the RIXS planes provides complementary information to the XAS technique and thus assist in gaining the overall picture about the states involved in the bonding process. HERFD XAS and RIXS are powerful tools for studying the electronic structure in an element–specific manner. The structure of various oxides and effect of dopants on the structure can be studied and insights into active species involved in various reactions can be revealed. The use of hard X-rays in XES is essential to establish structure-performance relationships for real catalysts and to translate the results from surface-science experiments, which are often done with single crystals under vacuum conditions and by means of soft X-rays or electrons. The dynamism in the structure of catalysts after interaction with reactants and adsorbates can be apprehended successfully by means of HERFD XAS and RIXS. The site selective EXAFS is beneficial in probing the structure of specific catalyst elements present in certain sites, which can further help in resolving the queries about the active catalytic centres. The application of X-ray emission spectrometers at various beamlines of synchrotrons, the combination of XES and XAS to provide complementary information, and the involvement of theory to comprehend the experimental data in this field has attracted the interest of a large number of researchers in various fields. The development of setups that combine complementary methods and fast X-ray sources will open up a new era for the study of catalytic reactions. A much wider application of these methods is expected.

Acknowledgements

The authors would like to acknowledge Pieter Glatzel for valuable discussions and his help during beamtimes at ID 26, ESRF (European Synchrotron Radiation Facility), France. The authors also thank Swiss National Science Foundation for the financial grant. C. L. and J. A. V. B. are thankful for support from the MaMaSELF consortium (http://etudes.univ-rennes1.fr/mamaself).

References

1 (*a*) G. Ertl, *Adv. Catal.*, 1990, **37**, 213; (*b*) R. J. Farrauto and R. M. Heck, *Catal. Today*, 1999, **51**, 351; (*c*) P. T. Fanson, W. N. Delgass and J. Lauterbach, *J. Catal.*, 2001, **204**, 35; (*d*) M. Haruta and M. Date, *Appl. Catal., A*, 2001, **222**, 427; (*e*) P.-A. Carlsson, L. Oesterlund, P. Thormaehlen, A. Palmqvist, E. Fridell, J. Jansson and M. Skoglundh, *J. Catal.*, 2004, **226**, 422; (*f*) N. Lopez, T. V. W. Janssens, B. S. Clausen, Y. Xu, M. Mavrikakis, T. Bligaard and J. K. Nørskov, *J. Catal.*, 2004, **223**, 232.

2 (*a*) D. S. Newsome, *Catal. Rev. Sci. Eng.*, 1980, **21**, 275; (*b*) D. Andreeva, V. Idakiev, T. Tabakov and A. Andreev, *J. Catal.*, 1996, **158**, 354; (*c*) H. Sakurai, A. Ueda, T. Kobayashi and M. Haruta, *Chem. Commun.*, 1997, 271; (*d*) T. Bunluesin, R. J. Gorte and G. W. Graham, *Appl. Catal., B*, 1998, **15**, 107; (*e*) T. Tabakova, V. Idakiev, D. Andreeva and I. Mitov, *Appl. Catal., A*, 2000, **202**, 91; (*f*) M. Mokhtar, T. M. Salama and M. Ichikawa, *J. Colloid Interface Sci.*, 2000, **224**, 336; (*g*) S. Hilaire, X. Wang, T. Luo, R. J. Gorte and J. Wagner, *Appl. Catal., A*, 2001, **215**, 271; (*h*) Q. Fu, A. Weber and M. Flytzani-Stephanopoulos, *Catal. Lett.*, 2001, **77**, 87.

3 (*a*) G. C. Bond and P. A. Sermon, *J. Chem. Soc., Chem. Commun.*, 1973, 444b; (*b*) Z. Xu, F.-S. Xiao, S. K. Purnell, O. Alexeev, S. Kawi, S. E. Deutsh and B. C. Gates, *Nature*, 1994, **372**, 346; (*c*) P. Claus, A. Brückner, C. Mohr and H. Hofmeister, *J. Am. Chem. Soc.*, 2000, **122**, 11430; (*d*) Y. H. Niu, L. K. Yeung and R. M. Crooks, *J. Am. Chem. Soc.*, 2001, **123**, 6840; (*e*) A. Corma and P. Serna, *Science*, 2006, **313**, 332.

4 (*a*) M. A. Vannice, *J. Catal.*, 1975, **37**, 462; (*b*) M. Araki and V. Ponec, *J. Catal.*, 1976, **44**, 439; (*c*) R. A. Demmin and R. J. Gorte, *J. Catal.*, 1987, **105**, 373; (*d*) J. G. Xu and G. F. Froment, *AIChE J.*, 1989, **35**, 88; (*e*) R. A. Lemons, *J. Power Sources*, 1990, **29**, 251; (*f*) M. J. Kahlich, H. A. Gasteiger and R. J. Behm, *J. Catal.*, 1997, **171**, 93.

5 (*a*) C. Bianchi, F. Porta, L. Prati and M. Rossi, *Top. Catal.*, 2000, **13**, 231; (*b*) F. Porta, L. Prati, M. Rossi, S. Coluccia and G. Martra, *Catal. Today*, 2000, **61**, 165.

6 (*a*) B. Hammer and J. K. Nørskov, *Nature*, 1995, **376**, 238; (*b*) D. E. Ramaker and D. C. Koningsberger, *Phys. Rev. Lett.*, 2002, **89**, 139701; (*c*) A. L. Ankudinov, J. J. Rehr, J. J. Low and A. R. Bare, *Phys. Rev. Lett.*, 2002, **89**, 139702; (*d*) G. A. Somorjai and A. L. Marsh, *Philos. Trans. R. Soc. London, Ser. A*, 2005, **363**, 879.

7 D. C. Koningsberger and R. Prins, in *X-ray Absorption: Principles, Applications, Techniques of EXAFS, SEXAFS, and XANES*, Wiley, New York, 1988.

8 E. A. Stern, D. E. Sayers and F. W. Lytle, *Phys. Rev. B: Solid State*, 1975, **11**, 4836.

9 (*a*) D. C. Koningsberger, B. L. Mojet, G. E. van Dorssen and D. E. Ramaker, *Top. Catal.*, 2000, **10**, 143; (*b*) J. A. van Bokhoven, T. Ressler, F. M. F. de Groot and G. Knopp-Gericke, in *In situ Spectroscopy of Catalysts*, ed. B. M. Weckhuysen, American Scientific Publishers, California, 2004, p. 123.

10 (*a*) D. E. Ramaker, B. L. Mojet, M. T. G. Oostenbrink, J. T. Miller and D. C. Koningsberger, *Phys. Chem. Chem. Phys.*, 1999, **1**, 2293; (*b*) A. L. Ankudinov, J. J. Rehr, J. Low and S. R. Bare, *Phys. Rev. Lett.*, 2001, **86**, 1642; (*c*) M. K. Oudenhuijzen, J. A. van Bokhoven, J. T. Miller, D. E. Ramaker and D. C. Koningsberger, *J. Am. Chem. Soc.*, 2005, **127**, 1530; (*d*) N. Weiher, E. Bus, L. Delannoy, C. Louis, D. E. Ramaker, J. T. Miller and J. A. van Bokhoven, *J. Catal.*, 2006, **240**, 100; (*e*) E. Bus, D. E. Ramaker and J. A. van Bokhoven, *J. Am. Chem. Soc.*, 2007, **129**, 8094.

11 D. E. Ramaker and D. C. Koningsberger, *Phys. Chem. Chem. Phys.*, 2010, **12**, 5514.

12 (*a*) B. K. Teo and P. A. Lee, *J. Am. Chem. Soc.*, 1979, **101**, 2815; (*b*) J. J. Rehr, J. Mustre de Leon, S. I. Zabinsky and R. C. Albers, *J. Am. Chem. Soc.*, 1991, **113**, 5135; (*c*) A. Filipponi, A. DiCicco and C. R. Natoli, *Phys. Rev. B: Condens. Matter*, 1995, **52**, 15122.

13 P. Glatzel, L. Jacquamet, U. Bergmann, F. M. F. de Groot and S. P. Cramer, *Inorg. Chem.*, 2002, **41**, 3121.

14 (*a*) K. Hämäläinen, D. P. Siddons, J. B. Hastings and L. E. Berman, *Phys. Rev. Lett.*, 1991, **67**, 2850; (*b*) X. Wang, F. M. F. de Groot and S. P. Cramer, *Phys. Rev. B: Condens. Matter*, 1997, **56**, 4553.

15 (*a*) G. Materlik, C. J. Sparks and K. Fischer, in *Resonant Anomalous X-Ray Scattering: Theory and Applications*, North-Holland, Amsterdam, 1994; (*b*) D. L. Ederer and J. H. McGuire, in *Raman Emission by X-Ray Scattering*, World Scientific, Singapore, 1996; (*c*) J. Nordgren and E. Z. Kurmaev, *J. Electron Spectrosc. Relat.*

Phenom., 2000, **110–111**, 1; (*d*) A. Kotani and S. Shin, *Rev. Mod. Phys.*, 2001, **73**, 203; (*e*) N. Wassdahl, A. Nilsson, T. Wiell, H. Tillborg, L. C. Duda, J. Guo, N. Mårtensson, J. Nordgren, J. N. Andersen and R. Nyholm, *Phys. Rev. Lett.*, 1992, **69**, 812.
16 (*a*) P. Glatzel and U. Bergmann, *Coord. Chem. Rev.*, 2005, **249**, 65; (*b*) J. A. van Bokhoven, C. Louis. J. T. Miller, M. Tromp, O. V. Safonova and P. Glatzel, *Angew. Chem., Int. Ed.*, 2006, **45**, 4651; (*c*) O. V. Safonova, M. Tromp, J. A. van Bokhoven, F. M. F. de Groot, J. Evans and P. Glatzel, *J. Phys. Chem. B*, 2006, **110**, 16162.
17 P. Glatzel, J. Singh, K. O. Kvashnina and J. A. van Bokhoven, *J. Am. Chem. Soc.*, 2010, **132**, 2555.
18 (*a*) K. Siegbahn, C. Nordling, G. Johansson, J. Hedman, P. F. Heden, K. Hamrin, U. Gelius, T. Bergmark, L. O. Werme, R. Manne and Y. Baer, in *ESCA Applied to Free Molecules*, North-Holland, Amsterdam, 1969; (*b*) S. Hufner, in *Photoelectron Spectroscopy*, Springer-Verlag, Berlin, 1995; (*c*) N. Mårtensson and A. Nilsson, in *Applications of Synchrotron Radiation: High Resolution Studies of Molecules and Molecular Adsorbates*, ed. W. Eberhardt, Springer-Verlag, Berlin, 1995, vol. 35.
19 S. D. Kevan, in *Angle-Resolved Photoemission*, Elsevier, Amsterdam, 1992.
20 U. Bergmann, C. R. Horne, T. J. Collins, J. M. Workman and S. P. Cramer, *Chem. Phys. Lett.*, 1999, **302**, 119.
21 V. A. Safonova, L. N. Vykhodsteva, Y. M. Polukarov, O. V. Safonova, G. Smolentsev, M. Sikora, S. G. Eeckhout and P. Glatzel, *J. Phys. Chem. B*, 2006, **110**, 23192.
22 F. de Groot, *Chem. Rev.*, 2001, **101**, 1779.
23 F. Gel'mukhanov and H. Ågren, *Phys. Rep. Rev. Soc. Phys. Lett.*, 1999, **312**, 91.
24 P. Carra, M. Fabirizio and B. T. Thole, *Phys. Rev. Lett.*, 1995, **74**, 3700.
25 (*a*) W. A. Caliebe, C. C. Kao, J. B. Hastings, M. Taguchi, T. Uozumi and F. M. F. de Groot, *Phys. Rev. B: Condens. Matter Mater. Phys.*, 1998, **58**, 13452; (*b*) P. Glatzel, U. Bergmann, W. W. Gu, H. X. Wang, S. Stepanov, B. S. Mandimutsira, C. G. Riordan, C. P. Horwitz, T. Collins and S. P. Cramer, *J. Am. Chem. Soc.*, 2002, **124**, 9668; (*c*) P. Glatzel, U. Bergmann, J. Yano, H. Visser, J. H. Robblee, W. Gu, F. M. F. de Groot, G. Christou, V. L. Pecoraro, S. P. Cramer and V. K. Yachandra, *J. Am. Chem. Soc.*, 2004, **126**, 9946; (*d*) F. M. F. de Groot, P. Glatzel, U. Bergmann, P. A. van Aken, R. A. Barrea, S. Klemme, M. Hävecker, A. Knop-Gericke, W. M. Heijboer and B. M. Weckhuysen, *J. Phys. Chem. B*, 2005, **109**, 20751.
26 K. Hämäläinen, C. C. Kao, J. B. Hastings, D. P. Siddons, L. E. Berman, V. Stojanoff and S. P. Cramer, *Phys. Rev. B: Condens. Matter*, 1992, **46**, 14274.
27 (*a*) J. Singh, R. C. Nelson, B. C. Vicente, S. L. Scott and J. A. van Bokhoven, *Phys. Chem. Chem. Phys.*, 2010, **12**, 5668; (*b*) J. A. van Bokhoven, *Phys. Chem. Chem. Phys.*, 2010, **12**, 5502.
28 (*a*) G. van der Laan, B. T. Thole, G. A. Sawatzky and M. Verdaguer, *Phys. Rev. B: Condens. Matter*, 1988, **37**, 6587; (*b*) J. van Elp, G. Peng, B. G. Searle, S. Mitra-Kirtley, Y. H. Huang, M. K. Johnson, Z. H. Zhou, M. W. W. Adams, M. J. Maroney and S. P. Cramer, *J. Am. Chem. Soc.*, 1994, **116**, 1918; (*c*) H. X. Wang, C. Y. Ralston, D. S. Patil, R. M. Jones, W. Gu, M. Verhagen, M. Adams, P. Ge, C. Riordan, C. A. Marganian, P. Mascharak, J. Kovacs, C. G. Miller, T. J. Collins, S. Brooker, P. D. Croucher, K. Wang, E. I. Stiefel and S. P. Cramer, *J. Am. Chem. Soc.*, 2000, **122**, 10544.
29 F. M. F. de Groot, *J. Electron Spectrosc. Relat. Phenom.*, 1994, **67**, 529.
30 U. Bergmann, P. Glatzel, F. De Groot and S. P. Cramer, *J. Am. Chem. Soc.*, 1999, **121**, 4926.
31 (*a*) G. Peng, F. M. F. de Groot, K. Hämäläinen, J. A. Moore, X. Wang, M. M. Grush, J. B. Hastings, D. P. Siddons, W. H. Armstrong, O. C. Mullins and S. P. Cramer, *J. Am. Chem. Soc.*, 1994, **116**, 2914; (*b*) P. Glatzel, U. Bergmann, F. M. F. de Groot and S. P. Cramer, *Phys. Rev. B: Condens. Matter Mater. Phys.*, 2001, **64**, 045109.
32 K. Tsutsumi, H. Nakamori and K. Ichikawa, *Phys. Rev. B: Solid State*, 1976, **13**, 929.
33 (*a*) S. D. Gamblin and D. S. Urch, *J. Electron Spectrosc. Relat. Phenom.*, 2001, **113**, 179; (*b*) H. Visser, E. Anxolabehere-Mallart, U. Bergmann, P. Glatzel, J. H. Robblee, S. P. Cramer, J. J. Girerd, K. sauer, M. P. Klein and V. K. Yachandra, *J. Am. Chem. Soc.*, 2001, **123**, 7031; (*c*) S. A. Pizarro, P. Glatzel, H. Visser, J. H. Robblee, G. Christou, U. Bergmann and V. K. Yachandra, *Phys. Chem. Chem. Phys.*, 2004, **6**, 4864.
34 D. S. Urch, in *Electron Spectroscopy: Theory, Techniques, and Applications*, ed. C. R. Brundle and A. D. Baker, Academic Press, New York, 1979, vol. 3, pp. 1–39.
35 F. de Groot, *Coord. Chem. Rev.*, 2005, **249**, 31.
36 J. C. Fuggle and J. E. Inglesfield, in *Unoccupied Electronic States*, Springer-Verlag, Berlin, 1992.
37 P. Glatzel, M. Sikora and M. Fernandez-Garcia, *Eur. Phys. J. Spec. Top.*, 2009, **169**, 207.
38 F. M. F. de Groot, M. H. Krisch and J. Vogel, *Phys. Rev. B: Condens. Matter Mater. Phys.*, 2002, **66**, 195112.
39 J. Yano, Y. Pushkar, P. Glatzel, A. Lewis, K. Sauer, J. Messinger, U. Bergmann and V. Yachandra, *J. Am. Chem. Soc.*, 2005, **127**, 14974.
40 C. Lamberti, A. Zecchina, E. Groppo and S. Bordiga, *Chem. Soc. Rev.*, 2010, **39**, DOI: 10.1039/c0cs00117a.
41 (*a*) A. L. Ankudinov, B. Ravel, J. J. Rehr and S. D. Conradson, *Phys. Rev. B: Condens. Matter Mater. Phys.*, 1998, **58**, 7565; (*b*) A. L. Ankudinov, C. Bouldin, J. J. Rehr, J. Sims and H. Hung, *Phys. Rev. B: Condens. Matter Mater. Phys.*, 2002, **65**, 104107.
42 (*a*) R. Barth, R. Pitchai, R. L. Anderson and X. E. Verykios, *J. Catal.*, 1989, **116**, 61; (*b*) R. Barth and A. Ramachandran, *J. Catal.*, 1990, **125**, 467.
43 B. Hammer and J. K. Nørskov, *Surf. Sci.*, 1995, **343**, 211.
44 J. Singh, E. M. Alayon, M. Tromp, O. V. Safonova, P. Glatzel, M. Nachtegaal, R. Frahm and J. A. van Bokhoven, *Angew. Chem., Int. Ed.*, 2008, **47**, 9260.
45 J. A. Anderson, *J. Chem. Soc., Faraday Trans.*, 1992, **88**(8), 1197.
46 R. Burch and P. K. Loader, *Appl. Catal., A*, 1995, **122**, 169.
47 F. J. Gracia, L. Bollmann, E. E. Wolf, J. T. Miller and A. J. Kropf, *J. Catal.*, 2003, **220**, 382.
48 M. D. Ackermann, T. M. Pedersen, B. L. M. Hendriksen, O. Robach, S. C. Bobaru, I. Popa, C. Quiros, H. Kim, B. Hammer, S. Ferrer and J. W. M. Frenken, *Phys. Rev. Lett.*, 2005, **95**, 255505.
49 R. Burch and P. K. Loader, *Appl. Catal., B*, 1994, **5**, 149.
50 S. Yang, A. M. Valiente, M. B. Gonzalez, I. R. Ramos and A. G. Ruiz, *Appl. Catal., B*, 2000, **28**, 223.
51 (*a*) X. Su, P. S. Cremer, Y. R. Shen and G. A. Somorjai, *J. Am. Chem. Soc.*, 1997, **119**, 3994; (*b*) F. J. Gracia, S. Guerrero, E. E. Wolf, J. T. Miller and A. J. Kropf, *J. Catal.*, 2005, **233**, 372; (*c*) E. M. Alayon, J. Singh, M. Nachtegaal, M. Harfouche and J. A. van Bokhoven, *J. Catal.*, 2009, **263**, 228.
52 T. H. Lindstrom and T. T. Tsotsis, *Surf. Sci.*, 1985, **150**, 487.
53 J. Singh, M. Nachtegaal, E. M. C. Alayon, J. Stötzel and J. A. van Bokoven, *ChemCatChem*, 2010, **2**, 653.
54 M. E. Grass, Y. Zhang, D. R. Butcher, J. Y. Park, Y. Li, H. Bluhm, K. M. Bratlie, T. Zhang and G. A. Somorjai, *Angew. Chem., Int. Ed.*, 2008, **47**, 8893.
55 (*a*) W. M. Heijboer, P. Glatzel, K. R. Sawant, R. F. Lobo, U. Bergmann, R. A. Barrea, D. C. Koningsberger, B. M. Weckhuysen and F. M. F. de Groot, *J. Phys. Chem. B*, 2004, **108**, 10002; (*b*) A. Zecchina, M. Rivallan, G. Berlier, C. Lamberti and G. Ricchiardi, *Phys. Chem. Chem. Phys.*, 2007, **9**, 3483.
56 (*a*) G. I. Panov, A. S. Kharitonov and V. I. Sobolev, *Appl. Catal., A*, 1993, **98**, 1; (*b*) G. I. Panov, G. A. Sheveleva, A. S. Kharitonov, V. N. Romannikov and L. A. Vostrikova, *Appl. Catal., A*, 1992, **82**, 31.
57 (*a*) P. Marturano, L. Drozdova, G. D. Pirngruber, A. Kogelbauer and R. Prins, *Phys. Chem. Chem. Phys.*, 2001, **3**, 5585; (*b*) A. A. Battiston, J. H. Bitter, F. M. F. de Groot, A. R. Overweg, O. Stephan, J. A. van Bokhoven, P. J. Kooyman, C. van Der Spek, G. Vanko and D. C. Koningsberger, *J. Catal.*, 2003, **213**, 251.
58 K. A. Dubkov, N. S. Ovanesyan, A. A. Shteinman, E. V. Starokon and G. I. Panov, *J. Catal.*, 2002, **207**, 341.
59 (*a*) G. Berlier, G. Spoto, S. Bordiga, G. Ricchiardi, P. Fisicaro, A. Zecchina, I. Rossetti, E. Selli, L. Forni, E. Giamello and C. Lamberti, *J. Catal.*, 2002, **208**, 64; (*b*) S. Bordiga, R. Buzzoni,

F. Geobaldo, C. Lamberti, E. Giamello, A. Zecchina, G. Leofanti, G. Petrini, G. Tozzola and G. Vlaic, *J. Catal.*, 1996, **158**, 486.
60 (*a*) A. M. Ferretti, C. Oliva, L. Forni, G. Berlier, A. Zecchina and C. Lamberti, *J. Catal.*, 2002, **208**, 83; (*b*) G. Berlier, G. Spoto, P. Fisicaro, S. Bordiga, A. Zecchina, E. Giamello and C. Lamberti, *Microchem. J.*, 2002, **71**, 101.
61 M. Wilke, F. Farges, P. E. Petit, G. E. Brown and F. Martin, *Am. Mineral.*, 2001, **86**, 714.
62 J. Pérez-Ramírez, G. Mul, F. Kapteijn, J. A. Moulijn, A. R. Overweg, A. Doménech, A. Ribera and I. W. C. E. Arends, *J. Catal.*, 2002, **207**, 113.
63 D. P. Woodruff and T. A. Delchar, in *Modern Techniques of Surface Science*, Cambridge University Press, New York, 1986.
64 (*a*) A. Nilsson, H. Tillborg and N. Mårtensson, *Phys. Rev. Lett.*, 1991, **67**, 1015; (*b*) A. Nilsson, M. Weinelt, T. Wiell, P. Bennich, O. Karis, N. Wassdahl, J. Stöhr and M. Samant, *Phys. Rev. Lett.*, 1997, **78**, 2847.
65 A. Föhlisch, M. Nyberg, P. Bennich, L. Triguero, J. Hasselström, O. Karis, L. G. M. Pettersson and A. Nilsson, *J. Chem. Phys.*, 2000, **112**, 1946.
66 (*a*) M. Weinelt, N. Wassdahl, T. Wiell, O. Karis, J. Hasselström, P. Bennich, A. Nilsson, J. Stöhr and M. Samant, *Phys. Rev. B: Condens. Matter Mater. Phys.*, 1998, **58**, 7351; (*b*) L. Triguero, A. Föhlisch, P. Väterlein, J. Hasselström, M. Weinelt, L. G. M. Pettersson, Y. Luo, H. Ågren and A. Nilsson, *J. Am. Chem. Soc.*, 2000, **122**, 12310.
67 (*a*) S. S. Sung and R. Hoffman, *J. Am. Chem. Soc.*, 1985, **107**, 578; (*b*) B. Hammer, Y. Morikawa and J. K. Norskov, *Phys. Rev. Lett.*, 1996, **76**, 2141; (*c*) F. Delbecq and P. Sautet, *Phys. Rev. B: Condens. Matter Mater. Phys.*, 1999, **59**, 5142.
68 (*a*) S. Andersson and J. B. Pendry, *Phys. Rev. Lett.*, 1979, **43**, 363; (*b*) J. Stohr and R. Jaeger, *Phys. Rev. B: Condens. Matter*, 1982, **26**, 4111.
69 P. Bennich, T. Wiell, O. Karis, M. Weinelt, N. Wassdahl, A. Nilsson, M. Nyberg, L. G. M. Pettersson, J. Stöhr and M. Samant, *Phys. Rev. B: Condens. Matter Mater. Phys.*, 1998, **57**, 9274.
70 (*a*) A. Nilsson, P. Bennich, T. Wiell, N. Wassdahl, N. Mårtensson, J. Nordgren, O. Björneholm and J. Stöhr, *Phys. Rev. B: Condens. Matter*, 1995, **51**, 10244; (*b*) A. Föhlisch, J. Hasselström, P. Bennich, N. Wassdahl, O. Karis, A. Nilsson, L. Triguero, M. Nyberg and L. G. M. Pettersson, *Phys. Rev. B: Condens. Matter Mater. Phys.*, 2000, **61**, 16229.
71 (*a*) P. S. Bagus, K. Hermann and C. W. Bauschlicher, *J. Chem. Phys.*, 1984, **81**, 1966; (*b*) P. S. Bagus, K. Hermann and C. W. Bauschlicher, *Phys. Rev. B: Condens. Matter*, 1984, **80**, 4378.
72 (*a*) H. Johann, *Z. Phys.*, 1931, **69**, 185; (*b*) V. Stojanoff, K. Hämäläinen, D. Siddons, J. Hastings, L. Berman, S. Cramer and G. Smith, *Rev. Sci. Instrum.*, 1992, **63**, 1125; (*c*) U. Bergmann and S. P. Cramer, *Proc. SPIE*, 1998, **3448**, 198; (*d*) K. Sakurai and H. Eba, *Jpn. J. Appl. Phys.*, 1999, **1**, 650; (*e*) E. Welter, P. Machek, G. Dräger, U. Bruggmann and M. Froba, *J. Synchrotron Radiat.*, 2005, **12**, 448.
73 C. C. Kao, K. Hämäläinen, M. Krisch, D. P. Siddons, T. Oversluizen and J. B. Hastings, *Rev. Sci. Instrum.*, 1995, **66**, 1699.
74 (*a*) A. Mozzanica, A. Bergamaschi, R. Dinapoli, F. Gozzo, B. Henrich, P. Kraft, B. Patterson and B. Schmitt, *Nucl. Instrum. Methods Phys. Res., Sect. A*, 2009, **607**, 250; (*b*) E. Kleimenov, A. Bergamaschi, J. A. Van Bokhoven, M. Janousch, B. Schmitt and M. Nactegaal, *J. Phys. Conf. Ser.*, 2009, **190**, 012035.
75 (*a*) S. Hayakawa, S. Goto, T. Shoji, E. Yamada and Y. Gohshi, *J. Synchrotron Radiat.*, 1998, **5**, 1114; (*b*) B. Dickinson, G. T. Seidler, Z. W. Webb, J. A. Bradley, K. P. Nagle, S. M. Heald, R. A. Gordon and I. M. Chou, *Rev. Sci. Instrum.*, 2008, **79**, 123112.
76 (*a*) L. V. von Hamos, *J. Sci. Instrum.*, 1938, **15**, 87; (*b*) H. Hayashi, M. Kawata, R. Takeda, Y. Udagawa, Y. Watanabe, T. Takano, S. Nanao and N. Kawamura, *J. Electron Spectrosc. Relat. Phenom.*, 2004, **136**, 191.
77 S. Huotari, G. Vanko, F. Albergamo, C. Ponchut, H. Graafsma, C. Henriquet, R. Verbeni and G. Monaco, *J. Synchrotron Radiat.*, 2005, **12**, 467.
78 A. C. Thompson, D. T. Attwood, E. M. Gullikson, M. R. Howells, J. F. Kortright, A. L. Robinson, J. H. Underwood, K.-Je Kim, J. Kirz, I. Lindau, P. Pianetta, H. Winick, G. P. Williams and J. H. Scofield, in *X-ray Data Booklet*, ed. A. C. Thompson and D. Vaughan, 2001.

